PARTICLE SIZE DISTRIBUTIONS OBTAINED THROUGH UNFOLDING 2D SECTIONS: TOWARDS ACCURATE DISTRIBUTIONS OF NEBULAR SOLIDS IN THE ALLENDE METEORITE. P. A. Christoffersen[1], J. I. Simon[2], D. K. Ross[2,3], J. M. Friedrich[4,5], and J. N. Cuzzi[6]. [1]St. Lawrence University, Canton, NY 13617, [2]NASA Johnson Space Center, Houston, TX 77058 (Justin.I.Simon@NASA.gov), [3]Jacobs/ESCG, Houston, TX 77058, [4]Fordham University, Bronx, NY 10458, [5]American Museum of Natural History, New York, NY 10024, [6]NASA Ames, Moffett Field, CA 94035.

Introduction: Size distributions of nebular solids in chondrites suggest an efficient sorting of these early forming objects within the protoplanetary disk. The effect of this sorting has been documented by investigations of modal abundances of CAIs (e.g., [1-4]) and chondrules (e.g., [5-8]). Evidence for aerodynamic sorting in the disk is largely qualitative, and needs to be carefully assessed. It may be a way of concentrating these materials into planetesimal-mass clumps, perhaps 100's of ka after they formed. A key parameter is size/density distributions of particles (i.e., chondrules, CAIs, and metal grains), and in particular, whether the radius-density product ($r\times\rho$) is a better metric for defining the distribution than r alone [9]. There is no consensus between r versus $r\times\rho$ based models. Here we report our initial tests and preliminary results, which when expanded will be used to test the accuracy of current dynamical disk models.

Samples: Allende, a CV3 oxidized carbonaceous chondrite contains nebular components, including a diversity of chondrules and refractory inclusions (Fig. 1A,B). NIST 1019b is a well-characterized particle size standard [10] that contains glass beads with diameters ranging from ~750 to 2450 μm (Fig. 1C,D).

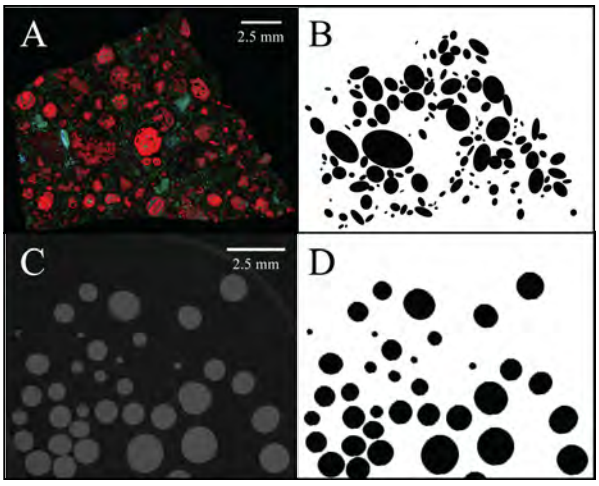

Figure 1. A) X-ray chemical map of Allende, with Mg, Ca, and Al as red, green, and blue. B) Best fit ellipses defined by ImageJ for just porphyritic chondrules from A. C) An example radial section of the NIST 1019b particle size standard imaged by x-ray tomography [10]. D) Best fit ellipses defined by ImageJ of glass beads from C.

Methods: The Allende meteorite was cut into ~cm thick slabs and broken into fragments that could be made into one inch epoxy rounds. One fragment was sawed into four serial sections spaced ~1.2 mm apart. The sections were polished using a series of grit sizes down to 1 μm for SEM analysis.

We took x-ray maps of the Allende sample using a JEOL 7600 Field Emission SEM with a silicon drift detector. Images were taken at 15 kV, 30 nA, with a 90 μm aperture. The maps were taken at ~150x magnification in which each pixel represents ~3 μm These maps were stitched together to form a large montage of Allende to quantify the abundance and composition of the different nebular solids. Mg, Ca, and Al x-ray maps were combined, and the particle distribution analyzed, using the image mixing and particle counting functions of ImageJ software. Initially, objects measured within the x-ray maps have been grouped textrually (i.e., pophyritic, barred, radiating, etc.), but will ultimately be grouped by composition. Objects were measured for area using best fit ellipses. For simplicity we consider that the particles can be approximated by spheres and calculate an average sphere diameter from the major and minor ellipses axes measured for each. Diameters calculated in this manner match those determined from the circular area defined by the total number of pixels.

We counted particles (i.e., nebular components) in Allende by tracing each using Adobe Illustrator. Then by taking the population of outlines and running it through ImageJ's automatic particle counting. We obtained the area, and major and minor axes of each particle greater than ~20 μm in diameter (seen in Fig. 2).

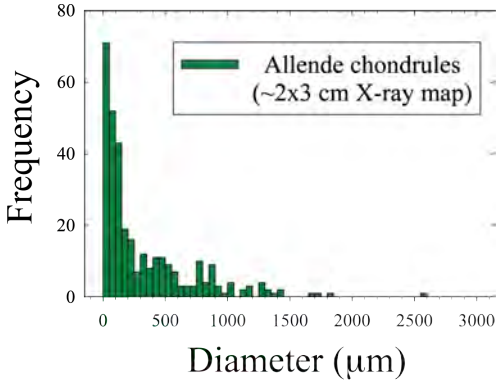

Figure 2. 2D size distribution of chondrules from ~15% of the x-ray maps collected for the Allende CV3 chondrite.

There are well-known sampling effects which cause the observed property $N_A(d)$, the number of particle sections or profiles, of diameter d per unit area, to differ from the more fundamental, desired quantity $N_V(D)$, the number of spheres of diameter D per unit

volume (e.g., [11]). Specifically, sections tend to cut particles non-diametrically, diminishing the fraction at true diameter D and artificially increasing the fraction at all smaller diameters (Fig. 3). We have written an algorithm that works as a simple matrix inversion [12] designed to unfold the particle sections obtained from the 2D Allende data set, however to calibrate the algorithm it was first tested on the particle size standard NIST 1019b. This was done using x-ray microtomography data [11] from 2D tomographic slices through NIST 1019b, a cylinder of glass beads.

We counted the glass bead sizes in NIST 1019b in a manner similar to that for Allende. In our trials, glass beads were both hand counted, by drawing an ellipse around the bead and measuring that ellipse's area, major, and minor axes, and auto counted by ImageJ, respectively (Fig. 1C,D). The error of measurements taken by hand were determined empirically to be ~10%, which is similar to the uncertainty found by the several ways we determined diameter with the automated ImageJ data collection routine.

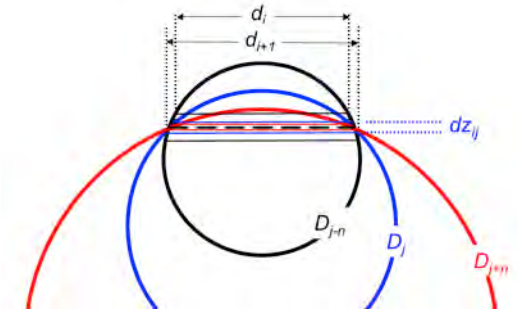

Figure 3. Graphical representation of the unfolding problem. The size distribution $N_A(d)$ and $N_V(D)$ are binned the same way, into a set of diameter bins with lower and upper boundaries at (d_{i-1}, d_i), with i = 1 representing the top end of the smallest particle size bin. For simplicity, we assume the spacing is regular, so $d_i = d_{i-1} + \Delta$, with $\Delta = D_{max}/N$.

Results and Discussion: The NIST 1019b standard was sampled near both the "top" and the "bottom" (sampling was made at intervals of 19.5 and 195 μm). The experiment was designed to capture the particle distribution of the overall population and differential settling within the sample container. The actual distribution and sampled distributions are shown in Fig. 4A. Fig. 4B shows the data after it was processed through our unfolding algorithm. Our sampling does not resolve the narrow peak at ~800 μm. The peak is about 50 μm wide, less than the absolute measurement error in the diameter estimate at that size. The success of our unfolding algorithm can be seen by comparison of Fig. 4A,B from diameters of 0 to ≤800 mm where, after unfolding, all of the small diameters that reflect non-diametric slices through a large sphere have been corrected for (i.e., "Forbidden" sizes). The unfolded data (20-bin histogram) also resolves differential settling of smaller and larger size components. The first is shown clearly in the "top" subset of data at ~1000 μm and the second in the "bottom" subset of data at ~1200 μm.

Allende x-ray maps revealed distinct chondrules, CAIs, and matrix in great detail, but future image processing will be needed to quantatively resolve more subtle intensity (i.e., compositional) differences. Nevertheless, preliminary analysis of ~15% of the Allende data, shown in Fig. 2, demonstrate the general exponential decline of larger sizes (e.g., [13]). More data will be processed before meaningful density differences among nebular components can be made.

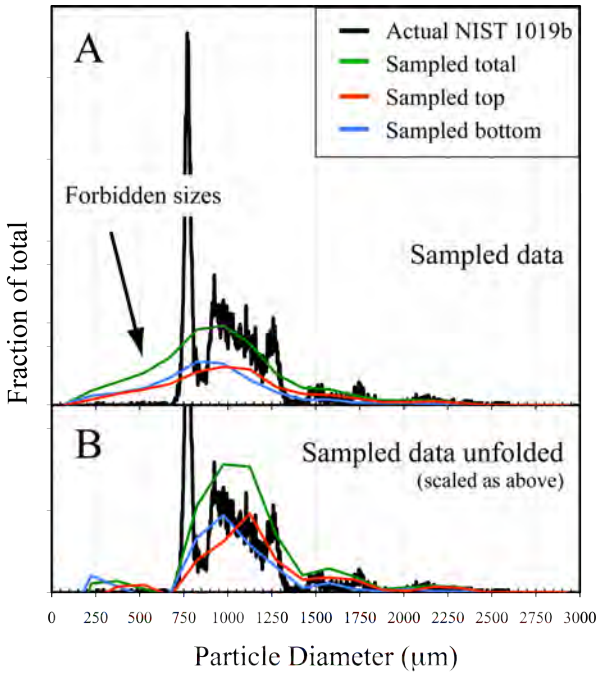

Figure 4. Top panel shows the line histogram data generated from measurements of NIST 1019b. Bottom slice data is in blue, top slice data is in red, total slice data is in green, and the accepted values are in black. Bottom panel shows data after unfolding. Note that the settling shows up clearly as does the modes of the larger particles.

References: [1] Aleon J. et al. (2002) *MPS, 37*, 1729-1755. [2] Brearley A.J. and Jones R.H. (1998) *MSA*, pp. 1-398. [3] Hezel D.C. et al. (2008) *MPS, 43,* 1879-1894. [4] Wurm G. and Krauss O. (2006) *Icarus, 180*, 487-495. [5] Cuzzi J.N. et al (2001) *APJ, 546*, 496-508. [6] Dodd R.T. (1976) *EPSL, 30,* 281--291. [7] Hughes D.W. (1978) *EPSL, 39*, 371-376. [8] Rubin A.E. and Grossman J.N. (1987) *Meteoritics 22*, 237-251. [9] Teitler, S.A. et al. (2010) *MPS* 45, 1124-1135. [10] Friedrich, J.M. et al. (2011) *PPSC, (submitted)*. [11] Eisenhour, D. 1996, *Meteoritics*, 31, 243-248. [12] Weibel E R (1980) *Academic Press*. [13] Cuzzi J. N., et al. (1996) in *Chondrules and the Protoplanetary Disk*, 35-43.